

Robust intralayer antiferromagnetism and tricriticality in the van der Waals compound VBr₃

Dávid Hovančík¹, Marie Kratochvílová¹, Tetiana Haidamak¹, Petr Doležal¹, Karel Carva¹, Anežka Bendová¹, Jan Prokleška¹, Petr Proschek¹, Martin Míšek², Denis I. Gorbunov³, Jan Kotek⁴, Vladimír Sechovský¹, and Jiří Pospíšil^{1,*}

¹Charles University, Faculty of Mathematics and Physics, Department of Condensed Matter Physics, Ke Karlovu 5, 121 16 Prague 2, Czech Republic

²Institute of Physics, Czech Academy of Sciences, Na Slovance 2, 182 21 Prague 8, Czech Republic

³Hochfeld-Magnetlabor Dresden (HLD-EMFL), Helmholtz-Zentrum Dresden-Rossendorf, 01328 Dresden, Germany

⁴Department of Inorganic Chemistry, Faculty of Science, Charles University, Hlavova 8, 128 40 Prague 2, Czech Republic



(Received 3 February 2023; accepted 29 August 2023; published 21 September 2023)

We studied magnetic states and phase transitions in the van der Waals antiferromagnet VBr₃ experimentally by specific heat and magnetization measurements of single crystals in high magnetic fields and theoretically by the density functional theory calculations focused on exchange interactions. The magnetization behavior mimics Ising antiferromagnets with magnetic moments pointing out-of-plane due to strong uniaxial magnetocrystalline anisotropy. The out-of-plane magnetic field induces a spin-flip metamagnetic transition of first-order type at low temperatures, while at higher temperatures, the transition becomes continuous. The first-order and continuous transition segments in the field-temperature phase diagram meet at a tricritical point. The magnetization response to the in-plane field manifests a continuous spin canting which is completed at the anisotropy field $\mu_0 H_{MA} \approx 27$ T. At higher fields, the two magnetization curves above saturate at the same value of magnetic moment $\mu_{\text{sat}} \approx 1.2 \mu_B/\text{f.u.}$, which is much smaller than the spin-only ($S = 1$) moment of the V³⁺ ion. The reduced moment can be explained by the existence of an unquenched orbital magnetic moment antiparallel to the spin. The orbital moment is a key ingredient of a mechanism responsible for the observed large anisotropy. The exact energy evaluation of possible magnetic structures shows that the intralayer zigzag antiferromagnetic (AFM) order is preferred, which renders the AFM ground state significantly more stable against the spin-flip transition than the other options. The calculations also predict that a minimal distortion of the Br ion sublattice causes a radical change of the orbital occupation in the ground state, connected with the formation of the orbital moment and the stability of magnetic order.

DOI: [10.1103/PhysRevB.108.104416](https://doi.org/10.1103/PhysRevB.108.104416)

I. INTRODUCTION

Van der Waals (vdW) magnets provide a natural platform for studying two-dimensional (2D) magnetism and its potential for advanced technologies like magneto-optics and spintronics [1–6]. Transition-metal trihalides, TX_3 ($T = \text{V}, \text{Cr}$; $X = \text{Cl}, \text{Br}, \text{I}$), form an important group of vdW magnets. VI_3 [7–9], CrBr_3 [10,11], and CrI_3 [12–15] become ferromagnetic (FM), whereas VBr_3 [7,16,17], VCl_3 [7], and CrCl_3 [18,19] are antiferromagnetic (AFM) at low temperatures. Historically, FM materials were considered more interesting from the point of view of applications, but recent discoveries show that AFMs may hold even larger potential for magnetism-based information storage and spintronics [20–22]. The TX_3 compounds are dimorphic, adopting the rhombohedral BiI_3 -type and the monoclinic AlCl_3 -type (or related types) layered crystal structures [8,9,13,14,16,23–25]. Both structure types are formed by stacking the X - T - X triple layers (further referred to as monolayers). The T -ion layer in the BiI_3 -type structure has a graphenelike honeycomb form of regular threefold symmetry. The monolayers are equidistantly

shifted, and the honeycomb network may be distorted in monoclinic structure [8,26]. The weak X - X vdW bond between neighboring monolayers allows their easy separation. This unique property, combined with the magnetic ordering within a monolayer at finite temperatures, provides a testing base for 2D magnetism and offers promising opportunities to fabricate 2D nanoelectronic devices [27,28].

The V trihalides undergo a structural phase transition from a high-temperature trigonal structure to the low-temperature monoclinic one at a temperature T_s ($\approx 79, 90,$ and 97 K for $\text{VI}_3, \text{VBr}_3,$ and VCl_3) [16,25]. The distortions of the β angle in VBr_3 ($90^\circ \rightarrow 90.55^\circ$) and VI_3 ($90^\circ \rightarrow 90.45^\circ$) are only slightly different. Kong *et al.* [16] reported VBr_3 AFM below $T_N = 26.5$ K with the magnetic moments perpendicular to the ab plane (out-of-plane direction). We mark this direction by the symbol c^* to distinguish it from the c axis, which is not perpendicular to the ab plane in the monoclinic structure. The recent publication [17] attributed the changes in Raman scattering spectra ~ 90 K to the structural transition associated with a decrease in the crystal-structure symmetry from $R\bar{3}$ to $C2/m$. The authors also reported minor hysteresis loops observed in low magnetic fields and ascribed them to a canted AFM order.

*jiri.pospisil@matfyz.cuni.cz

This paper is mainly devoted to aspects of VBr_3 physics not treated in previous studies presented in the literature. The experiments were focused primarily on the influence of the magnetic field on the structural and magnetic phases in VBr_3 , which can bring essential information on the mechanisms driving the specific phenomena. The structural-transition temperature T_s was found intact by magnetic fields contrary to the reduction of T_s of the isostructural ferromagnet VI_3 in the out-of-plane field ($H||c^*$) [24]. The observed dramatically different responses of T_N -related specific-heat anomalies and magnetization isotherms to the fields $H||c^*$ and $H\perp c^*$ reveal strong uniaxial magnetocrystalline anisotropy. VBr_3 , like other AFMs, undergoes a magnetic-field-induced AFM \rightarrow paramagnetic (PM) metamagnetic phase transition (MPT) at critical magnetic field H_c . We have observed a spin-flip transition in fields $H||c^*$ that is typical for an Ising-like anti-ferromagnet. In fields $H\perp c^*$, i.e., in the ab plane, a continuous spin canting has been found running from the lowest fields and completed around $\mu_0 H_c \approx 27\text{ T}$, which can be considered a reasonable estimate of the anisotropy field. Such a high value of the anisotropy field indicates the presence of a significant V orbital magnetic moment. The existence of orbital moment can also consistently explain the size of the saturated magnetic moment of $1.2 \mu_B/\text{f.u.}$ observed in high magnetic fields ($\mu_0 H_c > 55\text{ T}$). This value is much smaller than the spin-only value ($2 \mu_B$) of the magnetic moment expected for the V^{3+} ion with a quenched orbital moment.

A closer inspection of the evolution of specific heat and magnetization isotherms in $H||c^*$ reveals that the MPT at lower temperatures has a first-order transition character contrary to higher temperatures up to T_N , where the MPT becomes a continuous transition. This behavior is typical for AFMs with a tricritical point (TCP) that separates the first order and the continuous metamagnetic transition segments in the field-temperature (H - T) magnetic phase diagram [29]. The archetype of this unique phenomenon is FeCl_2 [29–31], also a layered vdW compound [32]. However, the tricriticality has not been reported in any other vdW AFM.

Previous first-principles calculations for VBr_3 predicted a strong FM intralayer superexchange interaction like in VI_3 [33]. This result suggests that the AFM structure should be composed of FM monolayers that are AFM coupled in the out-of-plane direction (layered AFM order), e.g., in the case of CrPS_4 [34]. The calculation results excluded only the Néel AFM order inside layers caused by the AFM nearest-neighbor interactions. Nevertheless, sufficiently strong negative exchange interactions between distant V next-nearest neighbors within the monolayer could also lead to more complex intralayer orders such as stripe or zigzag AFM order [35,36]. Magnetism at a honeycomb lattice is typically described by interactions up to third nearest neighbor (J_1 - J_2 - J_3 model). The zigzag AFM order has been identified in other quasi-2D systems on the honeycomb spin-lattice FePS_3 [37,38] and NiPS_3 [39,40]. The interlayer interaction was predicted to be an order of magnitude smaller than the intralayer one. Other studies were devoted only to the theoretical calculations of properties of VBr_3 monolayers [41,42].

The current state of understanding of the physics of the vdW AFM VBr_3 motivated us to focus this paper on the role of crystal structure details on exchange interactions and the

influence of the applied magnetic field on the magnetic states. To study the impact of crystal-structure details in determining the character of the exchange interactions and the magnetic ground state, we performed density functional theory (DFT) calculations. Spin-orbit coupling (SOC), which plays a vital role in the formation of the orbital moment, has been included. The calculations demonstrate that the ion network deformation is crucial for the stability of the AFM ordering of VBr_3 . Our findings contradict the previous assumption of layered AFM ordering since we have found that zigzag AFM order is energetically more favorable than FM order in layers. The predicted energy difference between this state and FM order is in agreement with the experimentally measured field needed to reorient spins. We have also shown that a particular displacement of Br atoms has a powerful impact on the ground-state orbital occupation and exchange interactions.

II. EXPERIMENTAL SECTION

A. Material synthesis and single-crystal growth

The single crystals of VBr_3 have been grown from pure elements (V 99.9%, Br_2 99.5%) using the chemical vapor transport method. This approach prevented contamination of the final product by residuals from precursors readily used to produce Br_2 , e.g., TeBr_4 used by Lyu *et al.* [17], in the reaction and transporting tube. First, a quartz tube with V metal powder kept at 300°C was evacuated overnight with simultaneous baking down to a vacuum of 10^{-7} mbar for proper degassing. Then the tube was filled with 6N argon gas and cooled to -60°C by dipping into an ethanol bath cooled by dry ice. Subsequently, the stoichiometric volume of Br_2 liquid was injected inside the frozen tube, where it instantly solidified. The continuously cooled tube with the mixture of V powder and solid Br_2 was then pre-evacuated by a Scroll pump and evacuated by a turbomolecular pump for 5 min with no signatures of Br_2 evaporation. Finally, the sealed quartz tube was inserted into a gradient furnace where a thermal gradient of $460/350^\circ\text{C}$ was kept for 2 weeks to transport all V metal from the hot part. The single crystals of the black-reflective color of several millimeter square dimensions have been obtained. The single crystals seem stable for several hours with no significant degradation effect. The desired 1:3 composition was confirmed by energy dispersive x-ray analysis. The crystallinity and orientation of the single crystals were confirmed by the Laue method showing sharp reflections. The rhombohedral c axis is perpendicular to the plane of platelike crystals.

B. Magnetization and specific-heat study

Specific heat was measured by the relaxation method and magnetization data with a vibrating sample magnetometer in magnetic fields up to 14 T using a Quantum Design PPMS 14T (Quantum Design Inc.) and up to 18 T with a Cryogenic cryomagnet (Cryogenic Ltd.). The Néel temperature T_N was determined from the temperature dependence of specific heat as the point of the balance of the entropy released at the phase transition. The field dependence of specific heat was measured point by point in a stable magnetic field. To probe the angular dependence of magnetization in the ac^* and ab planes (7 T),

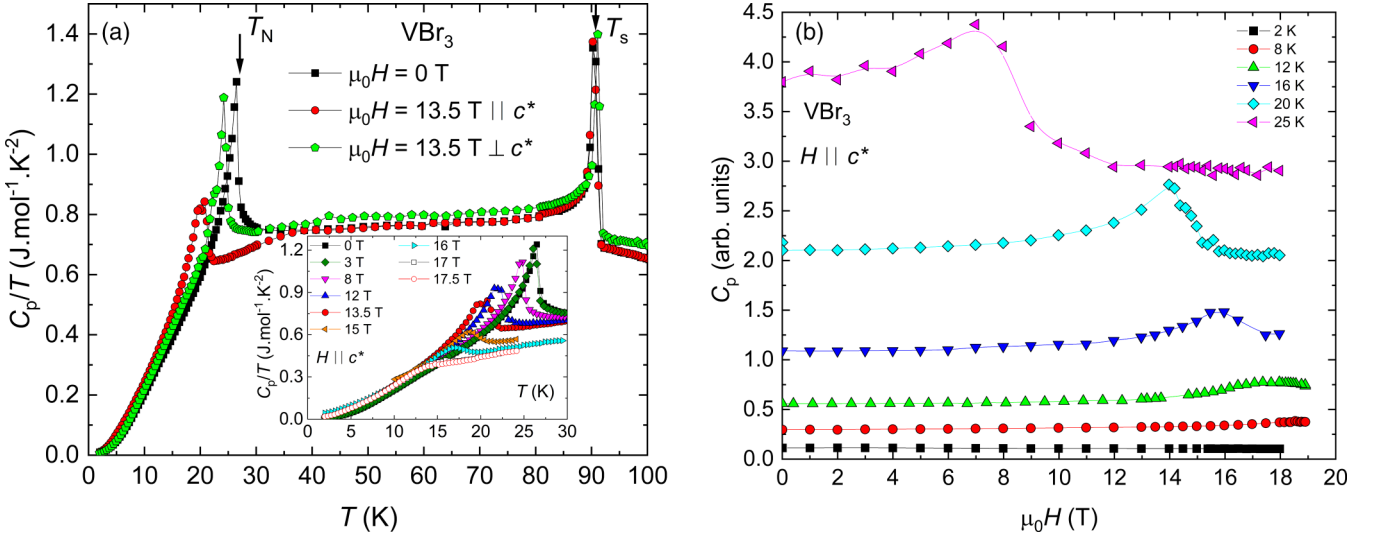


FIG. 1. (a) The temperature dependence of specific heat of VBr_3 in zero magnetic field (\blacksquare) and the field of 13.5 T applied parallel (\bullet) and perpendicular (\bullet) to c^* . The arrows mark the positions of T_N and T_s . The inset shows the variation of the T_N -related anomaly for the magnetic fields applied in the c^* direction. (b) The specific-heat isotherms of VBr_3 at selected temperatures for the magnetic field parallel to c^* .

we used a homemade rotator for MPMS 7T with a rotation axis orthogonal to the applied magnetic field. The magnetization in pulsed magnetic fields up to ~ 58 T was measured at the Dresden High Magnetic Field Laboratory using a high-field magnetometer [43] with a coaxial pick-up coil system. Absolute values of the magnetization were calibrated using data obtained in steady fields. The measurements in magnetic fields were performed for two perpendicular directions of the field: in the ab plane and perpendicular to the ab plane. The c axis in the monoclinic structure is not perpendicular to the ab plane. To avoid ambiguities, we use the symbol c^* for the direction perpendicular to the ab plane ($c^* \perp ab$ plane). In the trigonal structure, c^* is parallel to the c axis ($c^* \parallel c$). We also note that the single crystals are very thin and fragile plates moreover unstable in air and commonly used solvents or glues [44]. It complicated the preparation and fixation of the samples for various experimental methods and caused slight uncertainty of their final masses which resulted in deviation of calculated absolute values of the physical quantities with 5–10% error bar.

C. Theoretical calculations

DFT calculations employed the full-potential linear augmented plane-wave (APW) method, as implemented in the band structure program ELK [45]. SOC plays a crucial role in V trihalides. Therefore, it has been included in the calculations [46,47]. The generalized gradient approximation (GGA) parametrized by Perdew-Burke-Ernzerhof [48] has been used to perform geometrical relaxation of the structure. We have used local density approximation as the exchange-correlation potential to determine more subtle properties requiring high precision in energy as well as the exchange interactions and magnetic anisotropy energy since, with GGA, we have noticed numerical instabilities and convergence problems. These may be related to the presence of multiple local energy minima in the configurational space or maybe of the same origin as those found in the pseudopotential-based calculation of vdW

trisulfides [49]. Since the material is known to be a Mott insulator, we have included the effect of electron-electron correlations in terms of the Hubbard correction term $U = 4.3$ eV [50–52] acting on V $3d$ electrons. Double counting was treated in the fully localized limit. Similar DFT + U + SOC calculations have already successfully described the quasi-2D compound VI_3 [52]. The entire Brillouin zone has been sampled by $10 \times 10 \times 5$ k points, and the convergence with respect to k-mesh density has been verified. For total energy calculations, increased angular momentum cutoff of the expansion into spherical harmonics has been used with $l_{\text{max}} = 14$ for the APW functions and $l_{\text{maxo}} = 8$ for the muffin-tin density and potential. To evaluate the interlayer interaction J_L , a unit cell doubled in the z direction was used. Energies of calculated self-consistent ground states with forced FM and AFM interlayer alignment (LAFM) then allow us to calculate $J_L = E_{\text{FM}} - E_{\text{LAFM}}$ for different possible geometries, like the pressure dependence of J_L calculated already for VI_3 [51]. To compare the energies of the possible magnetic orderings inside the layer, we double the unit cell in one of the planar directions. The basis with 4 V atoms in the layer allows us to evaluate energies of AFM Néel, stripe, and zigzag orders as well as FM order [53].

III. RESULTS AND DISCUSSION

Two transitions were detected in specific-heat data [see Fig. 1(a)] in agreement with Kong *et al.* [16] and Lyu *et al.* [17]. The sharp peak at $T_s = 90$ K corresponds to the structural transition between the monoclinic and trigonal phases. The λ -shaped anomaly at $T_N = 26.5$ K indicates a second-order phase transition between the low-temperature AFM and PM states (AFM \leftrightarrow PM).

The structural phase transition is intact by magnetic fields up to 18 T [13.5 T data are shown in Fig. 1(a)] applied in both principal directions. This result contrasts with the significant field dependence of the corresponding structural phase transformation of isostructural vdW FM VI_3 in fields

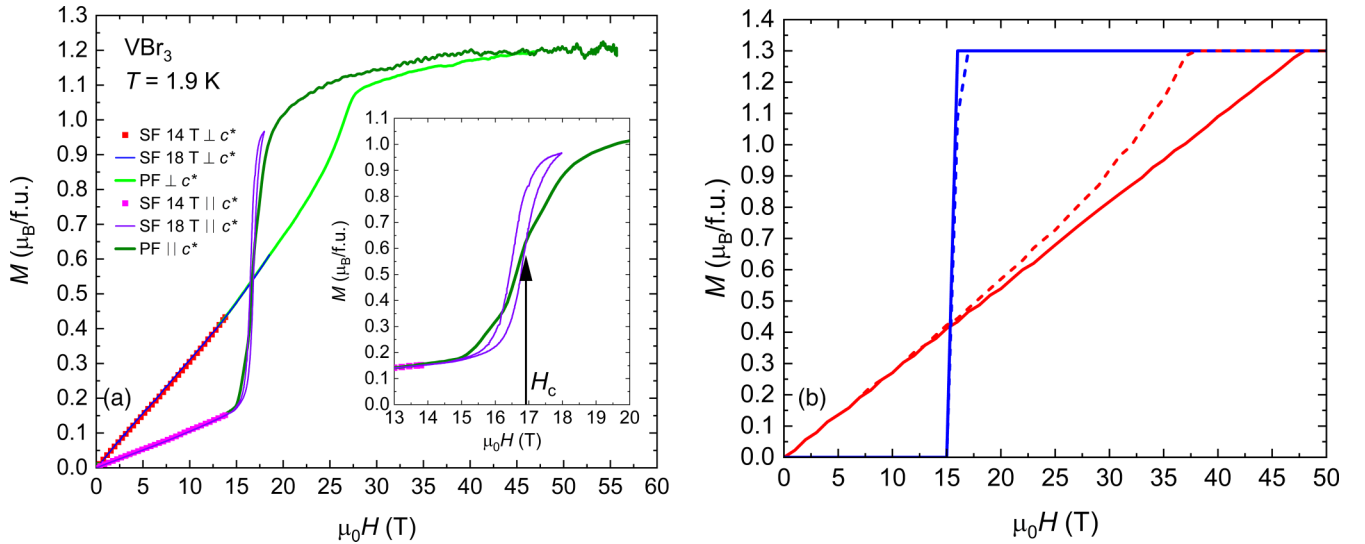


FIG. 2. (a) The magnetization isotherms of VBr_3 measured at 1.9 K in static fields (SFs) up to 18 T and pulsed fields (PFs) $H||c^*$ and $H\perp c^*$ up to 58 T. Inset: The detail of the plots for $H||c^*$ between 13 and 20 T. The arrow points to the critical field H_c . The absolute value of the calibrated magnetization isotherms can vary with an error bar $\pm 10\%$. (b) Stoner-Wohlfarth simulation. Plotted M along H per one site as a function of applied external field H , for H parallel to the easy axis (blue) or perpendicular to the easy axis (red). Solid lines are calculated according to the model assuming purely uniaxial anisotropy ($K_2 = 0$ meV), while calculations depicted with dashed lines include a higher-order term ($K_2 = 0.2$ meV).

parallel to c^* [24], which can be understood as a result of the FM correlations detected in Raman spectra [54], combined with strong magnetoelastic interaction. On the other hand, the applied magnetic field pushes the T_N -related anomaly in VBr_3 to lower temperatures and smears it out. These effects are much more pronounced for $H||c^*$. No sign of magnetic phase transition is detected in magnetic fields > 17.5 T.

Specific-heat isotherms measured in varying magnetic fields $H||c^*$ up to 18 T are shown in Fig. 1(b). A broad-peak anomaly on the $C_p(H)$ isotherm manifests the second-order metamagnetic transition (AFM \rightarrow PM) at temperatures from 12 K and T_N . For temperatures < 12 K, no anomaly is detected on the C_p vs H plot. That is consistent with C_p vs T data for $T < 12$ K in the inset of Fig. 1(a) which barely change with the applied magnetic field. Considering Maxwell's relation:

$$\left(\frac{\partial S}{\partial H}\right)_T = \left(\frac{\partial M}{\partial T}\right)_H, \quad (1)$$

this behavior indicates a negligible temperature dependence of magnetization in different magnetic fields for $T < 12$ K.

The 2 K $M(H)$ isotherms $H||c^*$ and $H\perp c^*$ in static fields up to 18 T are shown in Fig. 2(a). The $M(H)$ measured in $H\perp c^*$ remains linear up to 15 T and then becomes convex. The convexity is more pronounced with further increasing H . The increasing $H||c^*$ field induces a steep S-shaped increase in fields > 15.5 T with an inflection point at 16.9 T. This anomaly resembles a spin-flip transition typical for AFMs with strong uniaxial magnetocrystalline anisotropy. The observed field hysteresis $\mu_0\Delta H \approx 0.3$ T suggests a first-order metamagnetic transition.

To reveal the limits of the AFM phase stability in the H - T phase space, we employed pulsed magnetic fields up to 58 T. The 1.9 K $M(H)$ isotherms are displayed in Fig. 2(a). For

$H||c^*$, the S-shaped profile is broader than in static fields, most likely due to a slower reaction of the magnetic moments to the fast field pulse. The magnetization in fields above the transition gradually saturates to the final value of $1.2 \mu_B/\text{f.u.}$ at 58 T. The $M(H)$ curve for $H\perp c^*$ is linear, becoming convex > 20 T. The convexity increases with increasing H up to the inflection point at ≈ 23 T, where the AFM \rightarrow PM transition appears. Above 27 T, the magnetization gradually saturates and approaches the $H||c^*$ curve. Both $M(H)$ curves join > 40 T. The observed saturated moment of $1.2 \mu_B/\text{f.u.}$ is much lower than that expected for the V^{3+} spin-only magnetic moment ($2 \mu_B/\text{f.u.}$) [16,41,42,47,55–57]. It is worth noting that the experimentally observed saturated moment for VBr_3 compares well with that measured on the FM VI_3 single crystals in which a large V orbital magnetic moment has been recently confirmed by x-ray magnetic circular dichroism experiments [58]. This result, together with the observed strong magnetic anisotropy and large H_c fields are clear indications that the V ion in AFM VBr_3 also bears a significant orbital moment. The results of our anisotropy study and $H\perp c^*$ magnetization isotherms are shown in the Supplemental Material (SM) [59].

Magnetization isotherm simulations based on the Stoner-Wohlfarth model for the two sublattices have recovered some characteristics of the observed $M(H)$ curves at zero temperature. This model assumes two macroscopic moments representing the two spin sublattices described by unit moments \mathbf{m}_1 and \mathbf{m}_2 . These are coupled by an effective interaction J^* and subjected to external field \mathbf{H} and magnetic anisotropy [60]. The corresponding free energy expressed per one V atom is then given by

$$E = -J^* \mathbf{m}_1 \cdot \mathbf{m}_2 + E_{\text{AN}}(\mathbf{m}_1, \mathbf{m}_2) + \mathbf{H} \cdot (\mathbf{m}_1 + \mathbf{m}_2) \mu_{\text{sat}}. \quad (2)$$

Assuming uniaxial anisotropy with an easy axis and magnitude K_1 , we may rewrite the energies using the angles (θ_1, θ_2) between the two moments and the easy axis:

$$E_{\text{AN}}(\mathbf{m}_1, \mathbf{m}_2) = K_1 \cdot (\sin^2\theta_1 + \sin^2\theta_2). \quad (3)$$

The external magnetic field is applied in the direction given by unit vector h . We search for moment directions minimizing the free energy. The observable quantity is the projection of total magnetization to the direction of the field, denoted as M , per one V atom; it is given as (value $\mu_s = 1.3 \mu_B$ was used)

$$M = \mathbf{h} \cdot (\mathbf{m}_1 + \mathbf{m}_2)\mu_s. \quad (4)$$

The fact that the $M(H)$ experimentally observed in the $H||c^*$ regime almost reaches saturation after the sudden increase indicates that a spin flip has occurred [61]. This behavior can be reproduced in this model if $K_1 \sim J^*/2$ or higher. Here, we assumed $J^* = -1.2$ meV, $K_1 = 0.6$ meV, which provides good agreement with the experimentally observed dependence for $H||c^*$. However, for the $H \perp c^*$ curve, a slower approach to saturation is predicted, see Fig. 2(b). There can be many reasons for this, given the limitations of the model. As the next step, we have extended the model by including a higher-order anisotropy term $K_2 \cdot (\sin^4\vartheta_1 + \sin^4\vartheta_2)$ which is present in systems with hexagonal or rhombohedral symmetry [62]. These terms were found to strongly affect field-induced magnetization dynamics in AFMs despite their small value [63]. A calculation assuming $K_2 = 0.2$ meV leads to markedly improved agreement with the observed slope for high $H \perp c^*$ (compare solid and dotted curves in Fig. S5 in the SM [59]). This indicates that the specific behavior of $M(H)$ curves can be explained by the difference in the presence of anisotropy terms of fourth power in $\sin \theta$.

The experimentally observed nonzero slope for small $H||c^*$ could be ascribed to an inclination of the field from the easy axis or the high content of defects in samples. Since the angular dependence of magnetization (Fig. S3 in the SM [59]) shows that the c direction corresponds to the easy axis, the latter explanation is more plausible. We have tested the model for various values of K_1 , and inclinations of field direction from the easy-axis results are displayed in Fig. S4 in the SM [59]. The employed semiclassical spin dynamics does not capture the effect of quantum fluctuations. However, authors of a recent study performed also on the J_1 - J_2 - J_3 model for the honeycomb lattice found that quantum fluctuations are strongly suppressed for the case of $S = 1$, so that the boundaries between different phases are only slightly changed as compared with the classical solution [64]. Therefore, we do not expect it to affect the main conclusions drawn from the semiclassical approach. Quantum fluctuations in AFM V trihalides deserve further study.

Since there are indications of a significant orbital moment value in VBr_3 , we have examined how it could affect the $M(H)$ curve. A crucial contribution to magnetic anisotropy originates from crystal-field effects (magnetocrystalline anisotropy). This interacts with the orbital moment directly, but its effect is transferred to spin via the spin-orbit interaction (SOI). Therefore, a sizable orbital moment can justify the high anisotropy that we used in our model, although the total moment is predominantly of spin origin. Furthermore, we have considered it as an extension of our

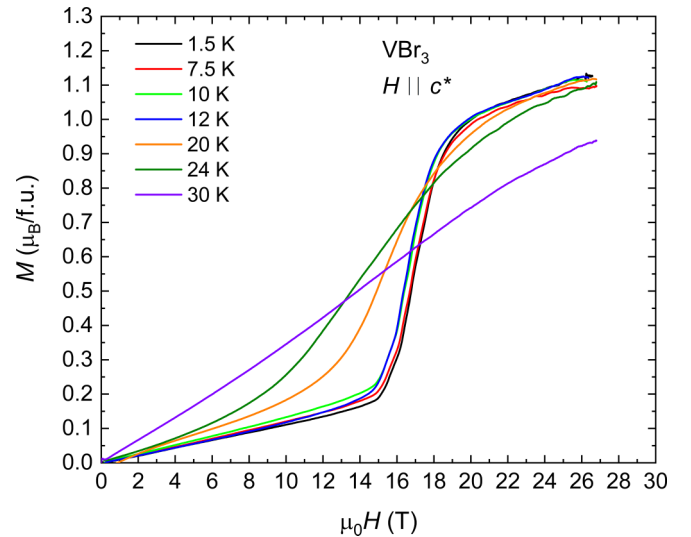


FIG. 3. The magnetization isotherms of VBr_3 measured at various temperatures in pulsed fields (PFs) for $H||c^*$ up to 27 T.

model where the spin and the orbital moment would be treated separately. However, within the expected values of the magnitude of SOI, this does not lead to a change of properties that would be observable. A detailed description is provided in the SM [59].

Figure 3 shows that the increasing temperature up to 12 K has a tiny effect on the first-order MPT (FOMPT) in the $M(H)$ curves in the field $H||c^*$. The critical field at 12 K is $\mu_0 H_c = 16.4$ T. This behavior reasonably matches the $C_p(H)$ dependence that is related via Maxwell's relation [see Eq. (1)]. The second-order (continuous) MPT (SOMPT) accompanied by magnetic fluctuations appears as a bump on the isothermal C_p vs H plot, while the anomaly disappears at FOMPT [Fig. 1(b)] because the released latent heat has vanished by the principle of the relaxation method in the PPMS apparatus (see an example in Ref. [65]). When inspecting Fig. 1(b) with decreasing temperature, we observe a smeared bump on the C_p vs H (a signature of SOMPT dependence) still at 12 K, whereas a FOMPT at this temperature is suggested by magnetization behavior. We take this as a sign of TCP proximity.

This evolution reflects the increasing influence of thermal fluctuations leading to the change of the character of the MPT to a continuous SOMPT at temperature interval $T_{\text{cp}} < T < T_N$. It indicates that VBr_3 belongs to the family of AFMs in which the MPT is a FOMPT at low temperatures and in the highest magnetic fields, whereas at higher temperatures and lower fields, a continuous (second-order), i.e., SOMPT is observed. The SOMPT in the zero-field limit is corroborated by the λ anomaly at T_N in the temperature dependence of specific heat, in clear contrast to rare systems with first-order AFM transition with the peaklike anomaly [66–69]. The FOMPT is characterized by a sudden reversal of AFM-coupled FM sublattice(s) to the direction of the applied field. The high-field ($H > H_c$) state is then characterized by field-polarized magnetic moments. It resembles an FM alignment of magnetic moments; however, it is a PM (not FM) state [29]. It is used to be called a polarized PM (PPM) regime [70].

TABLE I. The calculated Heisenberg exchange interactions J_i (in meV).

| Interaction | J_1 | J_2 | J_3 |
|-------------------|-------|-------|-------|
| 100 K structure | 1.87 | -0.57 | -0.46 |
| Relaxed structure | 1.76 | -0.33 | -1.04 |

The Ising AFM FeCl_2 [30,31] with competing FM and AFM exchange interactions is considered the archetype of this interesting family of materials. To retain the FOMPT > 0 K and to permit the occurrence of hysteresis at metamagnetic transition (MT), a FM intrasublattice exchange is necessary for a simple Ising system. The FM exchange in VBr_3 is documented by the Heisenberg exchange interactions in the third nearest-neighbor model, see Table I, where $J_1 > 0$. In such a case, a ratio $t^* = T_{\text{TCP}}/T_N \approx 0.45$ for VBr_3 is established and proportional to

$$\tau^* = 1 - \left(\frac{A}{3\Gamma} \right), \quad (5)$$

where A and Γ are molecular field coefficients [30].

The H - T phase diagram of VBr_3 for $H \parallel c^*$ is displayed in Fig. 4. The PM \leftrightarrow AFM phase transition line has two parts: a low-temperature part of FOMPTs and a high-temperature part of SOMPTs separated by the TCP [29,71] which we tentatively place at [12 K, 16.4 T] in the H - T phase diagram. Unfortunately, we do not have more M vs H and C_p vs H isotherms data measured at steady fields enabling us

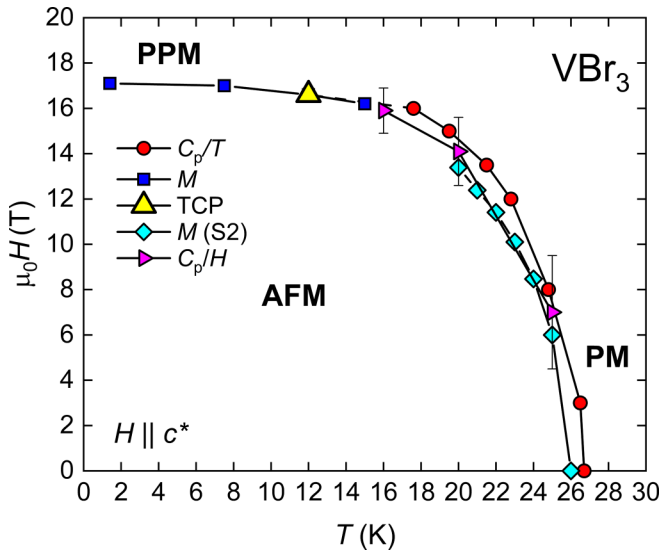


FIG. 4. The H - T phase diagram of VBr_3 for magnetic field applied along the c^* . The blue curve represents the inflection points on metamagnetic phase transition (MPT) in pulsed field data, the red curve the position of the anomaly in specific-heat data (C_p), the cyan curve represents the kink of MPT in steady-field data (see Fig. S1 in the SM [59]), and the magenta point shows the position of anomalies in field dependence of specific-heat data. The yellow point shows the estimated position of the tricritical point (TCP). The TCP is tentatively placed at $T_{\text{TCP}} = 12$ K, $\mu_0 H_{\text{TCP}} = 16.4$ T. $M(S2)$ represents data measured on a sample of lower quality (less stable in air) for comparison.

to determine T_{TCP} and H_{TCP} coordinates more precisely. The lack of experimental facilities providing steady fields within a reasonable T - H space prevents performing magnetization measurements for a reliable study of critical coefficients in the interesting case of a 2D AFM with a TCP.

We emphasize that VBr_3 is not a single non-Ising AFM with FOMPT and SOMPT segments in the H - T phase space separated by TCP. Analogous behavior is also found in some AFMs characterized by strong uniaxial anisotropy [71–73] as well as in one exhibiting strong orthorhombic anisotropy [74,75].

We have used first-principles calculation methods to evaluate the energies of the FM-ordered system, three plausible intralayer AFM orderings, and the layered AFM state. First calculations were performed for the lattice geometry determined by x-ray diffraction at 100 K, where the lattice parameters were found to be $a = 6.3711$ Å, $c = 18.3763$ Å, and the Br planes are placed at $h_{\text{Br}} = 0.07928$ c above (or below) the V planes [16]. Our calculations predict that the magnetic ground state has a zigzag AFM [Fig. 5(a)] order and not the suggested layered AFM structure consisting of FM ordered layers with antiparallel orientation between neighboring layers [33] [Fig. 5(b)].

All other considered AFM orders, including the layered AFM state, are energetically less favorable (Table II). Using calculated energies of magnetic configurations, one can map the problem to an effective Heisenberg Hamiltonian:

$$H = -\frac{1}{2} \sum_{i,j} J_{ij} s_i \cdot s_j, \quad (6)$$

where s_i is the unit vector corresponding to the i th spin in the system, J_{ij} is the exchange energy between the i th and j th spins, and the sums run over magnetic atoms in the system. Magnetism at a honeycomb lattice is efficiently described by the Heisenberg model with interactions up to the third nearest neighbor [J_1 - J_2 - J_3 model, schematically depicted in Fig. 6(b)]. Individual exchange interactions can be calculated from the calculated four energies of the four plausible magnetic order [76] and are shown in Table I. The energy difference between the AFM zigzag state and the FM state corresponds to the stability of the system with respect to a field-induced spin-flip transition. It can be denoted as $2J^*$, an effective interaction between the two AFM coupled sublattices (in the J_1 - J_2 - J_3 model, it equals $-J_1 - 4J_2 - 3J_3$). We find $J^* = -1.9$ meV per V atom. This finding appears to be consistent with the experimental knowledge about the presence of the AFM state and its stability, as the calculated J^* is rather close to the value we could use to simulate the experimentally observed spin-reorientation transition (Fig. 2) within the Stoner-Wohlfarth model.

Note that the magnetically ordered state is present only in the low-temperature structure below T_s . The low-temperature structure is only known to be slightly distorted, so that its symmetry is reduced to the monoclinic [22], but the structure details about anion positions are unknown. Therefore, as the next step, we performed geometrical relaxation of the atomic positions, starting from the monoclinically distorted structure. The optimized structure exhibits the following significant changes compared with the original one: (i) a decrease

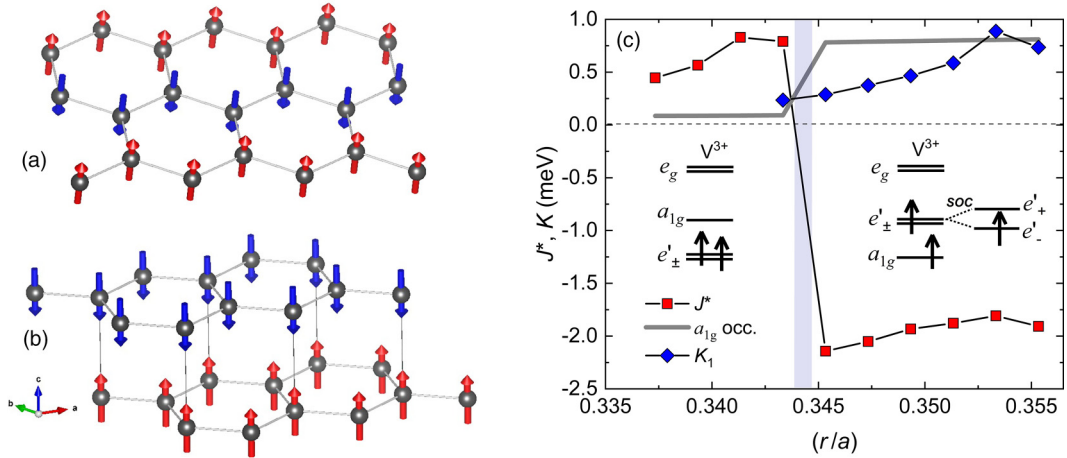


FIG. 5. (a) The predicted antiferromagnetic (AFM) structure of VBr_3 . Only a single layer of V^{3+} ions is displayed. The AFM structure consists of ferromagnetic (FM) zigzag chains coupled AFM within the plane. (b) Layered AFM structure (FM ordered layers with antiparallel orientation between neighboring layers) [33]. Two layers of V^{3+} ions are displayed, and lines in the vertical direction connect V ions stacked on top of each other (differing only in the z coordinate). (c) Calculated effective exchange J^* and anisotropy K_1 as a function of the distance r (in multiples of lattice parameter a). The occupation of the V^{3+} d states is calculated and schematically displayed in the diagrams.

of Br plane height h_{Br} by only $\approx 0.002c$, (ii) a slight planar shift of Br sites in the direction toward the midpoint between its two nearest V atoms, so that its distance r from the hollow site in the honeycomb lattice increases from the value of $r_m = 0.349a$ (measured at 100 K) to $r_{\text{opt}} = 0.353a$ [see Fig. 6(a)]. A similar distortion has been predicted by first-principles computational optimization in BiI_3 , but in the opposite direction, anions have moved toward the vacant point in the cation honeycomb lattice [77].

We have studied the effect of these deformations on the difference between FM and zigzag AFM order energies J^* . Changing the Br height h_{Br} does not introduce a significant change in the calculated exchange interactions to the extent suggested by the relaxation. The dependence of the effective exchange interactions J^* on the planar Br distortion [Fig. 6(a)] is shown in Fig. 5(c). The relaxed h_{Br} was included in these calculations. Note that the exchange varies only slowly with r (within numerical precision), while at a specific distance, a sudden change of the effective magnetic exchange occurs.

Like VI_3 , the electronic structure of VBr_3 may converge to two strikingly different solutions: a state with a quenched orbital moment, typical for $3d$ transition metals in a medium-strength crystal field, or a state with a high orbital moment. This problem is connected with the position of different

energy levels of trigonal symmetry electronic d orbitals in the ground state, particularly with the question of whether the a_{1g} orbital or one of the e'_g orbitals will be positioned above the Fermi level, as debated for VI_3 [46,47,58,78]. If the a_{1g} orbital is unoccupied, e'_g has to be fully occupied, and the orbital moment would be suppressed. For the spin moment, the calculations predict values close to $2 \mu_{\text{B}}/\text{f.u.}$, in agreement with Hund's rules, but the experimental magnetic moment is $1.2 \mu_{\text{B}}/\text{f.u.}$ This sharp transition is associated with a change in the occupation of different electronic orbitals in the ground state. For $r < r_{\text{crit}}$ states, fully occupied e'_g are preferred, while a state with a_{1g} occupied turns out to be favorable for r above this threshold value $r_{\text{crit}} = 0.344a$.

A correct Br position has to be used to obtain the correct ground state in calculations. For $r = r_{\text{opt}}$, our calculations predict a sizeable magnetocrystalline anisotropy 0.89 meV , a value that is reasonably close to that we have used to describe the field-induced spin flip within the Stoner-Wohlfahrt model. For example, the assumption of the so-called ideal position (with $r = a/3$) [77] would lead to a different magnetic order as well as an electronic structure. A compression of r by only

TABLE II. The calculated energies of magnetic structures relative to the zigzag AFM.

| Type of magnetic structure | Relative total energies E (meV/f.u.) | |
|----------------------------|--|-------------------|
| | 100 K structure | Relaxed structure |
| AFM zigzag | 0 | 0 |
| FM | +1.91 | +2.66 |
| Layered AFM | +1.65 | +2.09 |
| AFM stripe | +3.26 | +4.87 |
| AFM Néel | +6.04 | +4.81 |

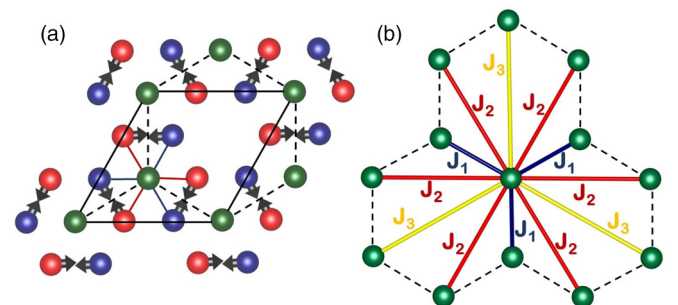


FIG. 6. (a) VBr_3 lattice plane, predicted relaxation is shown. (b) Heisenberg model with interactions up to the third nearest neighbor (J_1 - J_2 - J_3).

$\sim 3\%$ from its optimal value is sufficient to overcome r_{crit} and reach this different state. Our calculations also predict easy-plane preference for that situation, together with significant orbital reoccupation for moment orientation in-plane. The state predicted for $r < r_{\text{crit}}$ does not correspond to current observations, but it could be reached by the application of pressure or if specific phononic modes would be significantly occupied.

A zigzag AFM magnetic structure was also predicted in vdW AFM FePS₃. The VBr₃ magnetization loops significantly differ from those of FePS₃ where specific magnetization plateaus (cascades) were detected [53,79]. These occur due to a special combination of exchange interaction values that favor a situation with partially flipped moments within a small range of applied fields, where for example, six moments in a unit cell point in one direction and two moments in the opposite direction [79]. Only a simple spin-flip transition was found in VBr₃; therefore, based on the suggested models, we suppose the simple out-of-plane zigzag intralayer AFM structure as displayed in Fig. 5(a) without preference for intermediate partially flipped states.

IV. CONCLUSIONS

We have grown high-quality single crystals of VBr₃ by chemical vapor transport directly from pure elements. In this paper, we address the character of AFM and phase transitions by measuring specific heat and magnetization in static magnetic fields up to 18.5 T and pulsed fields up to 58 T. The structural transition at $T_s = 90$ K remains intact by magnetic fields, which is in contrast with the decrease of T_s in the isostructural ferromagnet VI₃. Here, T_N was found to decrease with increasing magnetic field much faster for the out-of-plane field than for the in-plane-direction field. The magnetization response to the magnetic field is strongly anisotropic. A first-order metamagnetic spin-flip transition to PPM occurs at $\mu_0 H_c = 16.9$ T in the out-of-plane field at 2 K. This transition remains first order at temperatures up to 12 K. At higher temperatures up to T_N , the AFM \rightarrow PM SOMPT occurs at lower fields. These phenomena are observed in some Ising AFMs with strong uniaxial anisotropy and competing AFM and FM interactions. Results of this study suggest VBr₃ to be a member of this group of materials with TCP at $\approx [12 \text{ K}, 16.4 \text{ T}]$. Further experiments that we do

not have available are needed to determine the coordinates of TCP precisely and determine the dimensionality of the system in terms of critical coefficients. High steady-field (at least up to 20 T) magnetization and electrical transport measurements are desirable. VBr₃ seems to be the only vdW AFM except the archetype FeCl₂ in which tricriticality has been reported.

The in-plane magnetization curve represents continuous spin canting toward the PM state with spin moments fully oriented along the applied field in fields > 27 T (at 2 K). The saturated magnetic moment observed in fields > 50 T $\mu_{\text{sat}} \approx 1.2 \mu_B/\text{f.u.}$ is much smaller than the spin-only moment ($2 \mu_B$) of a V^{3+} ion. This indicates the existence of a significant orbital magnetic moment, which partly compensates for the spin moment, like the VI₃ case.

Our calculations predict that the magnetic structure in VBr₃ is based on the intralayer AFM order in the form of a zigzag pattern. We have also found that the relaxation of Br atomic position plays an important role in the electronic structure calculations and the resulting magnetic properties of the system. A small change in the distances of Br atoms from the hollow site in the honeycomb lattice leads to a sudden redistribution of orbital occupation in the ground state. This suggests that phonon modes leading to a similar displacement would be strongly coupled to magnetic order here.

ACKNOWLEDGMENTS

This paper is a part of the research project GAČR 21–06083S which is financed by the Czech Science Foundation and Project GAUK 938220 financed by the Charles University Grant Agency. The single-crystal growth, characterization, and experiments in steady magnetic fields were carried out in the Materials Growth and Measurement Laboratory [80], which is supported within the program of Czech Research Infrastructures (Project No. LM2023065). This project was also supported by OP VVV Project MATFUN under Grant No. CZ.02.1.01/0.0/0.0/15_003/0000487. We acknowledge the support from HLD at HZDR, a member of the EMFL where the measurements in pulsed magnetic fields were done. This paper was supported by the Ministry of Education, Youth and Sports of the Czech Republic through the e-INFRA CZ (ID: 90140). We appreciate fruitful discussions with K. Výborný. The authors are also indebted to Dr. Ross H. Colman for critical reading and correcting of the manuscript.

-
- [1] D. L. Duong, S. J. Yun, and Y. H. Lee, *ACS Nano* **11**, 11803 (2017).
 - [2] K. S. Burch, D. Mandrus, and J. G. Park, *Nature (London)* **563**, 47 (2018).
 - [3] W. Zhang, P. K. J. Wong, R. Zhu, and A. T. S. Wee, *InfoMat* **1**, 479 (2019).
 - [4] M. Gibertini, M. Koperski, A. F. Morpurgo, and K. S. Novoselov, *Nat. Nanotechnol.* **14**, 408 (2019).
 - [5] M. C. Wang, C. C. Huang, C. H. Cheung, C. Y. Chen, S. G. Tan, T. W. Huang, Y. Zhao, Y. F. Zhao, G. Wu, Y. P. Feng *et al.*, *Ann. Phys.* **532**, 1900452 (2020).
 - [6] S. Kumari, D. K. Pradhan, N. R. Pradhan, and P. D. Rack, *Emergent Materials* **4**, 827 (2021).
 - [7] J. A. Wilson, C. Maule, and J. N. Tothill, *J. Phys. C Solid State Phys.* **20**, 4159 (1987).
 - [8] S. Son, M. J. Coak, N. Lee, J. Kim, T. Y. Kim, H. Hamidov, H. Cho, C. Liu, D. M. Jarvis, P. A. C. Brown *et al.*, *Phys. Rev. B* **99**, 041402(R) (2019).
 - [9] T. Kong, K. Stolze, E. I. Timmons, J. Tao, D. R. Ni, S. Guo, Z. Yang, R. Prozorov, and R. J. Cava, *Adv. Mater.* **31**, 1808074 (2019).
 - [10] H. Yoshida, J. Chiba, T. Kaneko, Y. Fujimori, and S. Abe, *Physica B* **237** 525 (1997).

- [11] L. D. Jennings and W. N. Hansen, *Phys. Rev.* **139**, A1694 (1965).
- [12] J. F. Dillon and C. E. Olson, *J. Appl. Phys.* **36**, 1259 (1965).
- [13] M. A. McGuire, H. Dixit, V. R. Cooper, and B. C. Sales, *Chem. Mater.* **27**, 612 (2015).
- [14] H. Wang, V. Eyert, and U. Schwingenschlogl, *J. Phys.: Condens. Matter* **23**, 116003 (2011).
- [15] W. B. Zhang, Q. Qu, P. Zhu, and C. H. Lam, *J. Mater. Chem. C* **3**, 12457 (2015).
- [16] T. Kong, S. Guo, D. Ni, and R. J. Cava, *Phys. Rev. Mater.* **3**, 084419 (2019).
- [17] B. Lyu, L. Wang, Y. Gao, S. Guo, X. Zhou, Z. Hao, S. Wang, Y. Zhao, L. Huang, J. Shao *et al.*, *Phys. Rev. B* **106**, 085430 (2022).
- [18] B. Kuhlow, *Phys. Status Solidi A* **72**, 161 (1982).
- [19] C. Starr, F. Bitter, and A. R. Kaufmann, *Phys. Rev.* **58**, 977 (1940).
- [20] T. Jungwirth, X. Marti, P. Wadley, and J. Wunderlich, *Nat. Nanotechnol.* **11**, 231 (2016).
- [21] P. Němec, M. Fiebig, T. Kampftrath, and A. V. Kimel, *Nat. Phys.* **14**, 229 (2018).
- [22] L. Šmejkal, A. H. Macdonald, J. Sinova, S. Nakatsuji, and T. Jungwirth, *Nat. Rev. Mater.* **7**, 482 (2022).
- [23] B. Morosin and A. Narath, *J. Chem. Phys.* **40**, 1958 (1964).
- [24] P. Doležal, M. Kratochvílová, V. Holý, P. Čermák, V. Sechovský, M. Dušek, M. Míšek, T. Chakraborty, Y. Noda, S. Son *et al.*, *Phys. Rev. Mater.* **3**, 121401(R) (2019).
- [25] M. Kratochvílová, P. Doležal, D. Hovančík, J. Pospíšil, A. Bendová, M. Dušek, V. Holý, and V. Sechovský, *J. Phys. Condens. Matter* **34**, 294007 (2022).
- [26] T. Marchandier, N. Dubouis, F. Fauth, M. Avdeev, A. Grimaud, J. M. Tarascon, and G. Rousse, *Phys. Rev. B* **104**, 014105 (2021).
- [27] P. V. Pham, S. C. Bodepudi, K. Shehzad, Y. Liu, Y. Xu, B. Yu, and X. Duan, *Chem. Rev.* **122**, 6514 (2022).
- [28] Y. Li, B. Yang, S. Xu, B. Huang, and W. Duan, *ACS Appl. Electron. Mater.* **4**, 3278 (2022).
- [29] E. Strykowski and N. Giordano, *Adv. Phys.* **26**, 487 (1977).
- [30] I. S. Jacobs and P. E. Lawrence, *Phys. Rev.* **164**, 866 (1967).
- [31] D. P. Landau, *Phys. Rev. Lett.* **28**, 449 (1972).
- [32] M. A. McGuire, *Crystals* **7**, 121 (2017).
- [33] L. Liu, K. Yang, G. Y. Wang, and H. Wu, *J. Mater. Chem. C* **8**, 14782 (2020).
- [34] Y. Peng, S. Ding, M. Cheng, Q. Hu, J. Yang, F. Wang, M. Xue, Z. Liu, Z. Lin, M. Avdeev *et al.*, *Adv. Mater.* **32**, 2001200 (2020).
- [35] J. B. Fouet, P. Sindzingre, and C. Lhuillier, *Eur. Phys. J. B* **20**, 241 (2001).
- [36] E. Rastelli, A. Tassi, and L. Reatto, *Physica B+C* **97**, 1 (1979).
- [37] D. Lançon, H. C. Walker, E. Ressouche, B. Ouladdiaf, K. C. Rule, G. J. McIntyre, T. J. Hicks, H. M. Rønnow, and A. R. Wildes, *Phys. Rev. B* **94**, 214407 (2016).
- [38] K. Kurosawa, S. Saito, and Y. Yamaguchi, *J. Phys. Soc. Jpn.* **52**, 3919 (1983).
- [39] D. Lançon, R. A. Ewings, T. Guidi, F. Formisano, and A. R. Wildes, *Phys. Rev. B* **98**, 134414 (2018).
- [40] A. R. Wildes, V. Simonet, E. Ressouche, G. J. McIntyre, M. Avdeev, E. Suard, S. A. J. Kimber, D. Lançon, G. Pepe, B. Moubaraki *et al.*, *Phys. Rev. B* **92**, 224408 (2015).
- [41] S. Tomar, B. Ghosh, S. Mardanya, P. Rastogi, B. S. Bhadoria, Y. S. Chauhan, A. Agarwal, and S. Bhowmick, *J. Magn. Magn. Mater.* **489**, 165384 (2019).
- [42] J. X. Sun, X. Zhong, W. W. Cui, J. M. Shi, J. Hao, M. L. Xu, and Y. W. Li, *Phys. Chem. Chem. Phys.* **22**, 2429 (2020).
- [43] Y. Skourski, M. D. Kuz'Min, K. P. Skokov, A. V. Andreev, and J. Wosnitzer, *Phys. Rev. B* **83**, 214420 (2011).
- [44] M. Kratochvílová, K. Uhlířová, M. Míšek, V. Holý, J. Zázvorka, M. Veis, J. Pospíšil, S. Son, J. G. Park, and V. Sechovský, *Mater. Chem. Phys.* **278**, 125590 (2022).
- [45] <http://elk.sourceforge.net/>.
- [46] L. M. Sandratskii and K. Carva, *Phys. Rev. B* **103**, 214451 (2021).
- [47] K. Yang, F. Fan, H. Wang, D. I. Khomskii, and H. Wu, *Phys. Rev. B* **101**, 100402 (2020).
- [48] J. P. Perdew, K. Burke, and M. Ernzerhof, *Phys. Rev. Lett.* **77**, 3865 (1996).
- [49] T. Y. Kim and C.-H. Park, *Nano Lett.* **21**, 10114 (2021).
- [50] V. I. Anisimov, F. Aryasetiawan, and A. I. Lichtenstein, *J. Phys.: Condes. Matter* **9**, 767 (1997).
- [51] J. Valenta, M. Kratochvílová, M. Míšek, K. Carva, J. Kaštil, P. Doležal, P. Opletal, P. Čermák, P. Proschek, K. Uhlířová *et al.*, *Phys. Rev. Mater.* **103**, 054424 (2021).
- [52] V. I. Anisimov, J. Zaanen, and O. K. Andersen, *Phys. Rev. B* **44**, 943 (1991).
- [53] A. R. Wildes, D. Lançon, M. K. Chan, F. Weickert, N. Harrison, V. Simonet, M. E. Zhitomirsky, M. V. Gvozdkikova, T. Ziman, and H. M. Rønnow, *Phys. Rev. B* **101**, 024415 (2020).
- [54] D. Hovančík, D. Repčec, F. Borodavka, C. Kadlec, K. Carva, P. Doležal, M. Kratochvílová, P. Kužel, S. Kamba, V. Sechovský *et al.*, *J. Phys. Chem. Lett.* **13**, 11095 (2022).
- [55] C. J. Ballhausen, *Introduction to Ligand Field Theory* (McGraw-Hill Book Co., New York, 1962).
- [56] Y. Liu, M. Abeykoon, and C. Petrovic, *Phys. Rev. Res.* **2**, 013013 (2020).
- [57] M. An, Y. Zhang, J. Chen, H. M. Zhang, Y. J. Guo, and S. Dong, *J. Phys. Chem. C* **123**, 30545 (2019).
- [58] D. Hovančík, J. Pospíšil, K. Carva, V. Sechovský, and C. Piamonteze, *Nano Lett.* **23**, 1175 (2023).
- [59] See Supplemental Material at <http://link.aps.org/supplemental/10.1103/PhysRevB.108.104416> for results of magnetocrystalline anisotropy study of VBr₃ compound by angular dependence of magnetization; extended results of specific heat, steady, and pulsed-field magnetization study; and extra theoretical calculations supporting the conclusions concerning the magnetic structure of VBr₃.
- [60] R. Skomski, *Simple Models of Magnetism* (Oxford University Press, Oxford, 2008).
- [61] S. Dong, J. M. Liu, S. W. Cheong, and Z. F. Ren, *Adv. Phys.* **64**, 519 (2015).
- [62] L. D. Landau, E. M. Lifshitz, and L. P. Pitaevskii, *Electrodynamics of Continuous Media* (Butterworth-Heinemann, Oxford, 1984).
- [63] A. N. Bogdanov, A. V. Zhuravlev, and U. K. Rößler, *Phys. Rev. B* **75**, 094425 (2007).
- [64] J. Merino and A. Ralko, *Phys. Rev. B* **97**, 205112 (2018).
- [65] J. Pospíšil, M. Míšek, M. Diviš, M. Dušek, F. R. de Boer, L. Havela, and J. Custers, *J. Alloys Compd.* **823**, 153485 (2020).

- [66] D. Hovančík, M. Kratochvílová, P. Doležal, A. Bendová, J. Pospíšil, and V. Sechovský, *J. Solid State Chem.* **316**, 123580 (2022).
- [67] J. J. Huntzicker and E. F. Westrum, *J. Chem. Thermodyn.* **3**, 61 (1971).
- [68] A. Mori, Y. Miura, H. Tsutsumi, K. Mitamura, M. Hagiwara, K. Sugiyama, Y. Hirose, F. Honda, T. Takeuchi, A. Nakamura *et al.*, *J. Phys. Soc. Jpn.* **83**, 024008 (2014).
- [69] N. S. Sangeetha, S. Pakhira, Q.-P. Ding, L. Krause, H.-C. Lee, V. Smetana, A.-V. Mudring, B. B. Iversen, Y. Furukawa, and D. C. Johnston, *Proc. Natl. Acad. Sci. USA* **118**, e2108724118 (2021).
- [70] W. Knafo, R. Settai, D. Braithwaite, S. Kurahashi, D. Aoki, and J. Flouquet, *Phys. Rev. B* **95**, 014411 (2017).
- [71] J. Valenta, F. Honda, M. Vališka, P. Opletal, J. Kaštil, M. Míšek, M. Diviš, L. Sandratskii, J. Prchal, and V. Sechovský, *Phys. Rev. B* **97**, 144423 (2018).
- [72] T. N. Haidamak, J. Valenta, J. Prchal, M. Vališka, J. Pospíšil, V. Sechovský, J. Prokleška, A. A. Zvyagin, and F. Honda, *Phys. Rev. B* **105**, 144428 (2022).
- [73] F. Honda, J. Valenta, J. Prokleška, J. Pospíšil, P. Proschek, J. Prchal, and V. Sechovský, *Phys. Rev. B* **100**, 014401 (2019).
- [74] D. Hovančík, A. Koriki, A. Bendová, P. Doležal, P. Proschek, M. Míšek, M. Reiffers, J. Prokleška, J. Pospíšil, and V. Sechovský, *Phys. Rev. B* **105**, 014436 (2022).
- [75] J. Pospíšil, Y. Haga, Y. Kohama, A. Miyake, K. Shinsaku, T. Naoyuki, M. Vališka, P. Proschek, J. Prokleška, V. Sechovsky *et al.*, *Phys. Rev. B* **98**, 014430 (2018).
- [76] T. Olsen, *J. Phys. D: Appl. Phys.* **54**, 314001 (2021).
- [77] H. Yorikawa and S. Muramatsu, *J. Phys.: Condens. Matter* **20**, 325220 (2008).
- [78] H. Lane, E. Pachoud, J. A. Rodriguez-Rivera, M. Songvilay, G. Xu, P. M. Gehring, J. P. Attfield, R. A. Ewings, and C. Stock, *Phys. Rev. B* **104**, L020411 (2021).
- [79] K. Okuda, K. Kurosawa, and S. Saito, *High Field Magnetization Process in FePS₃* (North-Holland, Amsterdam, 1983).
- [80] <http://mgml.eu>.